

The second-order intrinsic Wiedemann-Franz law

Ying-Fei Zhang¹, Zhi-Fan Zhang², Zhen-Gang Zhu^{3,1,*} and Gang Su^{4,5†}

¹ School of Physical Sciences, University of Chinese Academy of Sciences, Beijing 100049, China.

² Interdisciplinary Center for Theoretical Physics and Information Sciences (ICTPIS), Fudan University, Shanghai 200433, China.

³ School of Electronic, Electrical and Communication Engineering,
University of Chinese Academy of Sciences, Beijing 100049, China.

⁴ Institute of Theoretical Physics, Chinese Academy of Sciences, Beijing 100190, China.

⁵ Kavli Institute for Theoretical Sciences, University of Chinese Academy of Sciences, Beijing 100190, China.

In recent years, the nonlinear anomalous thermal Hall effect has attracted substantial attention. In this paper, we carry out a theoretical exploration of the intrinsic anomalous thermal Hall and Nernst effect that is induced by the thermal Berry connection polarizability. This effect is independent of the relaxation time and can be present in antiferromagnets possessing \mathcal{PT} symmetry. Additionally, we put forward a second-order intrinsic Wiedemann-Franz law, which represents the ratio of the second-order intrinsic thermal conductivity coefficient to the second-order intrinsic electrical conductivity coefficient. When analyzed within a four-band \mathcal{PT} symmetric Dirac model, we observe that the second-order intrinsic thermal conductivity coefficient is linearly proportional to the second-order intrinsic electrical conductivity coefficient, and the second-order intrinsic Wiedemann-Franz law is characterized by the chemical potential μ in the low-temperature regime. These findings provide significant implications for experimental verification.

I. INTRODUCTION

The Berry curvature (BC) Ω [1, 2], likened to a magnetic field within the parameter space, plays a central role in modern quantum physics. It is found that the detailed distribution of BC in momentum space has profound impact on realistic physical world especially leading to topological nonlinearity. There exist the ohmic and Hall-type nonlinear currents [3]. The ohmic current can be segmented into the extrinsic Drude current and the intrinsic current contributed by Berry connection polarizability (BCP) [4–7]. The Hall type currents are instigated by Berry curvature dipole (BCD) and BCP. Sodemann and Fu [8] postulated that in systems with time reversal symmetry (\mathcal{T}) and broken inversion symmetry (\mathcal{P}), the second-order Hall conductivity is proportional to BCD and exhibits a linear dependence on the relaxation time τ , thereby signifying its extrinsic nature. A diverse array of materials, such as bilayer or few-layer WTe_2 [9, 10], the ferroelectric-like metal LiOsO_3 [11], Weyl semimetals [12–14], and others [15–17], have been recognized as manifesting this phenomenon. On the other hand, the gauge-invariant correction to the Berry connection [18–21] also gives rise to a nonlinear anomalous Hall effect (NAHE) that is independent of τ . This intrinsic effect emanates from BCP [20–23] and preponderates in parity-inversion time-reversal (\mathcal{PT})-symmetric materials since BCD vanishes due to symmetry constraints [24]. It is sensitively contingent upon the Néel vector [20, 21], presenting a means for the electrical measurement of antiferromagnetic materials. When the driving electric field is supplanted by a thermal flux, the associated intrinsic thermal transport is consequently associated with thermal Berry connection polarizability (TBCP) [25], which represents an intrinsic thermal transport induced by nontrivial topological properties.

Inspired by NAHE, the nonlinear anomalous thermal Hall effect (NATHE) and the nonlinear anomalous Nernst effect (NANE) have also attracted significant attention. These effects inherently give rise to corresponding anomalous electric, thermal, and thermoelectric transport coefficients, which have been the subject of extensive research [26–34]. The relationships among these coefficients are encapsulated within the Wiedemann-Franz (WF) law and the Mott relation [35–38]. According to linear response theory [39], the WF law displays the ratio of electrical conductivity σ_{ab} to thermal conductivity κ_{ab} at low temperature as $\kappa_{ab}/\sigma_{ab} = LT$, where $L = \frac{1}{3} \left(\frac{k_B \pi}{e} \right)^2$ is the Lorentz number. Meanwhile, the Mott relation stipulates $\alpha_{ab} = eLT \frac{\partial \sigma_{ab}}{\partial \mu}$ with Nernst coefficient α_{ab} and chemical potential μ . Recently, it is proposed that there exist nonlinear WF law and the Mott relation induced by BCD [38], in which the second-order WF law is given $\sigma_{abc} \propto \frac{\partial \kappa_{abc}}{\partial \mu}$, and the second-order Mott relation reads $\sigma_{abc} \propto \alpha_{abc}$ at low temperature, where σ_{abc} , κ_{abc} and α_{abc} stand for the second-order conductivity, thermal conductivity and Nernst coefficient, respectively. However, when TBCP prevails in \mathcal{PT} -symmetric materials, the above BCD-induced second-order WF law and Mott relation will be vanishing, and the intrinsic topological nonlinear thermoelectric responses will be leading order, indicating the elaborate and complex interaction between the nontrivial topology of energy bands and the transverse nonlinear Hall-like transport.

In this work, we deduce formulas for the second-order intrinsic thermal and charge currents in the presence of a temperature gradient. These formulas are independent of the relaxation time and are preponderant in \mathcal{PT} -symmetric materials. Subsequently, we present the second-order intrinsic WF law, which represents a ratio between the second-order intrinsic thermal conductivity coefficient and the second-order intrinsic electrical conductivity coefficient. To enhance our understanding of the impact of TBCP on nonlinear transport, we investigate a four-band Dirac model with \mathcal{PT} symmetry. It is observed that when this intrinsic effect is dominant, the

* zgzhu@ucas.ac.cn

† gsu@ucas.ac.cn

second-order intrinsic WF law $\kappa_{abc} \sim \mu\sigma_{abc}$, which is determined by μ .

II. THEORETICAL FORMULATION

The Hamiltonian including the effect of temperature gradient ∇T is $\hat{H}_T = \hat{H}_0 + \hat{H}'$ [40], where \hat{H}_0 is the Hamiltonian without perturbation, and

$$\hat{H}' = -\frac{1}{2} \left[\hat{H}_0, \hat{\mathbf{r}} \right]_+ \cdot \mathbf{E}_T, \quad (1)$$

where the subscript $+$ means anti-commutation, $\hat{\mathbf{r}}$ is position operator, and the thermal field \mathbf{E}_T represents temperature gradient $\mathbf{E}_T = -\frac{\nabla T}{T}$, where $\nabla = \partial/\partial\mathbf{r}$. Using time-independent perturbation theory, the first-order $\mathcal{O}(\mathbf{E}_T)$ perturbed Bloch state [25] reads

$$|\tilde{u}_n(\mathbf{k})\rangle = |u_n(\mathbf{k})\rangle - \sum_{l \neq n} \frac{\mathbf{E}_T \cdot \mathcal{A}_{ln}(\mathbf{k})}{2} \frac{\varepsilon_{n,\mathbf{k}} + \varepsilon_{l,\mathbf{k}}}{\varepsilon_{n,\mathbf{k}} - \varepsilon_{l,\mathbf{k}}} |u_l(\mathbf{k})\rangle, \quad (2)$$

where $|u_n(\mathbf{k})\rangle$ is the unperturbed Bloch state, $\mathcal{A}_{ln}(\mathbf{k}) = \langle u_l(\mathbf{k}) | i\nabla_{\mathbf{k}} | u_n(\mathbf{k}) \rangle$ is the interband Berry connection, where $\nabla_{\mathbf{k}} = \partial/\partial\mathbf{k}$. $\varepsilon_{n,\mathbf{k}}$ is the unperturbed band energy and n, l are band indexes.

The perturbed band energy $\tilde{\varepsilon}_{n,\mathbf{k}}$ is

$$\tilde{\varepsilon}_{n,\mathbf{k}} = \varepsilon_{n,\mathbf{k}} + \varepsilon_{n,\mathbf{k}}^{(1)} + \varepsilon_{n,\mathbf{k}}^{(2)}, \quad (3)$$

where the first-order $\mathcal{O}(\mathbf{E}_T)$ correction to the band energy vanishes [7, 18], i.e., $\varepsilon_{n,\mathbf{k}}^{(1)} = \langle u_n(\mathbf{k}) | \hat{H}' | u_n(\mathbf{k}) \rangle = 0$, and $\varepsilon_{n,\mathbf{k}}^{(2)}$ is proportional to \mathbf{E}_T^2 . The perturbed BC $\tilde{\Omega}_n(\mathbf{k})$ reads

$$\tilde{\Omega}_n(\mathbf{k}) = \Omega_n(\mathbf{k}) + \Omega_n^{(1)}(\mathbf{k}), \quad \Omega_n^{(1)}(\mathbf{k}) = \nabla_{\mathbf{k}} \times \mathcal{A}_n^{(1)}(\mathbf{k}), \quad (4)$$

where $\Omega_n(\mathbf{k})$ is the unperturbed BC, and $\Omega_n^{(1)}(\mathbf{k})$ is the first-order $\mathcal{O}(\mathbf{E}_T)$ correction of BC, $\mathcal{A}_n^{(1)}(\mathbf{k})$ is the first-order Berry connection, which effectively captures the band geometric quantity, and takes the form [25]

$$\mathcal{A}_{n,a}^{(1)}(\mathbf{k}) = \mathbb{G}_{n,ab}^T(\mathbf{k}) \mathbf{E}_{T,b}. \quad (5)$$

The Einstein summation for a and b is implicit, and indices a and b denote the Cartesian coordinates, $\mathbf{E}_{T,b}$ is the component of the thermal field \mathbf{E}_T in the direction b , $\mathbb{G}_n^T(\mathbf{k})$ is the TBCP tensor and its components are defined as

$$\mathbb{G}_{n,ab}^T(\mathbf{k}) = -\Re \sum_{l \neq n} \frac{(\varepsilon_{n,\mathbf{k}} + \varepsilon_{l,\mathbf{k}}) \mathcal{A}_{nl,a}(\mathbf{k}) \mathcal{A}_{ln,b}(\mathbf{k})}{\varepsilon_{n,\mathbf{k}} - \varepsilon_{l,\mathbf{k}}}. \quad (6)$$

With regard to the NAHE, the electric current expands into linear and nonlinear terms according to the electric field, $j_a^E = \sigma_{ab} E_b + \sigma_{abc} E_b E_c + \dots$. Considering the NATHE, the thermal current is expanded in powers of temperature gradient, $j_a^Q = \kappa_{ab}(-\nabla_b T) + \kappa_{abc}(-\nabla_b T)(-\nabla_c T) + \dots$. For the NANE, the electric current is expressed as a series expansion in terms of the temperature gradient, i.e. $j_a^N =$

$\alpha_{ab}(-\nabla_b T) + \alpha_{abc}(-\nabla_b T)(-\nabla_c T) + \dots$, where $\{a, b, c\} \in \{x, y, z\}$ represents the Cartesian coordinates. Symmetry constraints may prohibit linear response so that the nonlinear response predominates. Such as, when time-reversal symmetry \mathcal{T} is broken, the linear response dominates due to Onsager's reciprocity relations [41]; when \mathcal{T} is preserved but inversion symmetry \mathcal{P} is broken, the linear response vanishes, and the second-order response of the BCD mechanism becomes dominant [8]. However, when \mathcal{T} and \mathcal{P} are individually broken, while \mathcal{PT} symmetry is preserved, both the linear response and the BCD mechanism disappear, and the intrinsic second-order response of the (T)BCP mechanism becomes dominant [20, 21, 25], which is the main focus of our work.

A. Second-order intrinsic anomalous thermal Hall effect

The total anomalous thermal current $\mathbf{j}_{\text{total}}^Q$ can be decomposed into three components: \mathbf{j}_v^Q , \mathbf{j}_E^Q , and \mathbf{j}_T^Q . Specifically, \mathbf{j}_v^Q refers to the longitudinal thermal current caused by group velocity $\mathbf{v}_{\mathbf{k}}$ of carriers, while \mathbf{j}_E^Q is transverse thermal current driven by an external electric field \mathbf{E} and is influenced by the nontrivial Berry curvature $\Omega_n(\mathbf{k})$. In this paper, we focus on \mathbf{j}_T^Q , which is the transverse thermal current mediated by the nontrivial Berry curvature in the presence of ∇T with zero electromagnetic field, given by [42, 43]

$$\mathbf{j}_T^Q = -\frac{k_B^2 T}{\hbar} \nabla T \times \int [d\mathbf{k}] \sum_n \Omega_n(\mathbf{k}) \left[\beta^2 (\varepsilon_{n,\mathbf{k}} - \mu)^2 f_0^n + \frac{\pi^2}{3} - \ln^2(1 - f_0^n) - 2 \text{Li}_2(1 - f_0^n) \right], \quad (7)$$

where \times stands for cross product operation, $[d\mathbf{k}]$ stands for $d^D k / (2\pi)^D$, D is the dimension, the Fermi-Dirac distribution function is expressed as $f_0^n = 1/[1 + e^{\beta(\varepsilon_{n,\mathbf{k}} - \mu)}]$, with $\beta = \frac{1}{k_B T}$, and $\text{Li}_n(x) = \sum_{m=1}^{\infty} \frac{x^m}{m^n}$ is the polylogarithm function.

When considering the influence of ∇T on transport properties with \mathcal{PT} symmetry, the thermal current can be derived by substituting the expressions $\tilde{\varepsilon}_{n,\mathbf{k}}$ and $\tilde{\Omega}_n(\mathbf{k})$ from Eqs. (3) and (4) into Eq. (7). The second-order current is obtained by selectively collecting the terms proportional to $(\nabla T)^2$, and it is evident that only the first-order correction of Berry curvature $\Omega_n^{(1)}(\mathbf{k})$ contributes to the second-order intrinsic transverse thermal current, implying that the thermal current arises as a result of modulated TBCP. The response tensor κ_{abc} is defined by

$$j_{T,a}^{Q,(2)} = \kappa_{abc}(-\nabla_b T)(-\nabla_c T), \quad (8)$$

where the superscript (2) represents the second-order term, so does the following, and

$$\kappa_{abc} = \frac{k_B^2}{\hbar} \int [d\mathbf{k}] \sum_n \Lambda_{abc}^n(\mathbf{k}), \quad (9)$$

with integrand (see Appendix A 1)

$$\Lambda_{abc}^n(\mathbf{k}) = \epsilon_{ab}\partial_a\mathbb{G}_{n,bc}^T(\mathbf{k}) \left[\frac{(\varepsilon_{n,\mathbf{k}} - \mu)^2 f_0^n}{(k_B T)^2} + \pi^2/3 - \ln^2(1 - f_0^n) - 2\text{Li}_2(1 - f_0^n) \right], \quad (10)$$

where $\epsilon_{\alpha\beta}$ is Levi-Civita antisymmetric tensor, $\partial_a = \partial/\partial k_a$. It is seen that this second-order thermal Hall effect is independent of τ and only related to band structure.

B. Second-order intrinsic anomalous Nernst effect

The NANE refers to the generated transverse charge current by applied ∇T due to Berry curvature [44]

$$\mathbf{j}^N = -\frac{e}{\hbar}\nabla T \times \sum_m \int [d\mathbf{k}] \Omega_m(\mathbf{k}) S_m(\mathbf{r}, \mathbf{k}), \quad (11)$$

$S_m(\mathbf{r}, \mathbf{k}) = \frac{(\varepsilon_{m,\mathbf{k}} - \mu)}{T} f_0^m + k_B \ln(1 + e^{-\beta(\varepsilon_{m,\mathbf{k}} - \mu)})$ is entropy density. Analogous to the derivation of κ_{abc} , we can derive the Nernst-like current by substituting the expressions $\tilde{\varepsilon}_{n,\mathbf{k}}$ and $\tilde{\Omega}_n(\mathbf{k})$ from Eqs. (3) and (4) into Eq. (11), suggesting that the intrinsic Nernst current is generated due to TBCP. The second-order intrinsic Nernst-like current is denoted as

$$j_a^{N,(2)} = \alpha_{abc}(-\nabla_b T)(-\nabla_c T), \quad (12)$$

and the corresponding second-order Nernst coefficient α_{abc} can be simplified as (see Appendix A 2),

$$\alpha_{abc} = \frac{e}{\hbar T} \epsilon_{ab} \sum_m \int [d\mathbf{k}] \partial_a \mathbb{G}_{m,bc}^T(\mathbf{k}) S_m(\mathbf{r}, \mathbf{k}). \quad (13)$$

C. Second-order intrinsic Wiedemann-Franz law

By solving the Boltzmann equation, it is found that the second-order conductivity consists of three components [24, 45], $\sigma_{abc} = \sigma_{abc}^{\text{Drude}} + \sigma_{abc}^{\text{BCP}} + \sigma_{abc}^{\text{BCD}}$, in which $\sigma_{abc}^{\text{Drude}} = -\frac{e^3 \tau^2}{\hbar^3} \int [d\mathbf{k}] \partial_a \varepsilon_{n,\mathbf{k}} \partial_b \partial_c f_0^n$ [3] and $\sigma_{abc}^{\text{BCD}} = -\frac{\tau e^3}{\hbar^2} \epsilon_{abd} \int [d\mathbf{k}] \Omega_{n,d}(\mathbf{k}) \partial_c f_0^n$ [8] are both extrinsic contributions, related to τ^2 and τ respectively. In this study, we focus on the second intrinsic term [20, 21]

$$\sigma_{abc}^{\text{BCP}} = -\frac{e^2}{\hbar} \epsilon_{ab} \sum_m \int [d\mathbf{k}] \partial_a \mathbb{G}_{m,bc}^E(\mathbf{k}) f_0^m, \quad (14)$$

where $\mathbb{G}_{m,ab}^E(\mathbf{k})$ is the BCP tensor [18, 46],

$$\mathbb{G}_{m,ab}^E(\mathbf{k}) = 2e\Re \sum_{m' \neq m} \frac{\mathcal{A}_{mm',a}(\mathbf{k}) \mathcal{A}_{m',b}(\mathbf{k})}{\varepsilon_{m,\mathbf{k}} - \varepsilon_{m',\mathbf{k}}}. \quad (15)$$

Eq. (14) shows the ‘‘Fermi surface’’ effect for NAHE, where only the bands near Fermi energy contribute to the integration.

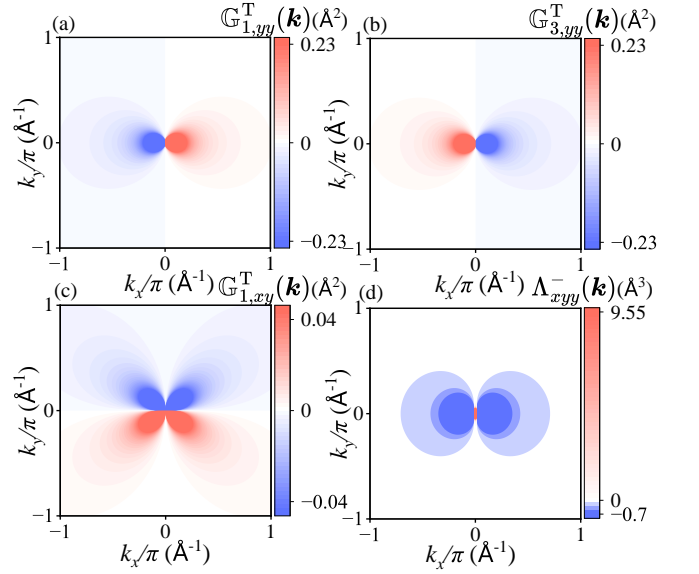


FIG. 1. (a) The contour plots of TBCP $\mathbb{G}_{1,yy}^T(\mathbf{k})$ in momentum space for the valence bands. (b) The contour plots of TBCP $\mathbb{G}_{3,yy}^T(\mathbf{k})$ in momentum space for the conduction bands. (c) The contour plots of TBCP $\mathbb{G}_{1,xy}^T(\mathbf{k})$ in momentum space for the valence bands. (d) The integrated function of thermal conductivity $\Lambda_{xyy}^-(\mathbf{k})$ for the valence bands. We set $v_x = v_y = 1$ eV $\dot{\text{A}}$, $\Delta = 40$ meV, $k_B T = 1$ meV ($T \sim 11.6$ K), $w/v_x = 0.4$.

At low temperature [30, 42], utilizing the Sommerfeld expansion [39], the second-order intrinsic WF law reads (see Appendix A)

$$\kappa_{abc} = -\frac{\pi^2 k_B^3 T}{3e^3} \frac{\epsilon_{ab} P_{a,bc}^T(\mu)}{\epsilon_{ab} P_{a,bc}^E(\mu)} \sigma_{abc}, \quad (16)$$

where $P_{a,bc}^T$ and $P_{a,bc}^E$ are defined as

$$P_{a,bc}^{\text{T(E)}}(\mu) = \frac{1}{k_B T(e)} \sum_n \int [d\mathbf{k}] \mathbb{G}_{n,bc}^{\text{T(E)}}(\mathbf{k}) \delta(\mu - \varepsilon_{n,\mathbf{k}}) \frac{\partial \varepsilon_{n,\mathbf{k}}}{\partial k_a}.$$

III. A MODEL STUDY

Under time reversal operation, $\Omega_n(\mathbf{k})$ is \mathcal{T} odd, wave vector \mathbf{k} is \mathcal{T} odd; while under the spatial inversion operation, $\Omega_n(\mathbf{k})$ is \mathcal{P} even, the wave vector \mathbf{k} is \mathcal{P} odd. We can know that $\mathcal{PT}\Omega_n(\mathbf{k}) = -\Omega_n(\mathbf{k}) = \Omega_n(\mathbf{k})$ in a \mathcal{PT} -symmetric system, which indicates the Berry curvature must be zero. Therefore, the Berry curvature $\Omega_n(\mathbf{k})$ vanishes in materials that preserve \mathcal{PT} symmetry, implying that linear and second-order responses contributed by BC are forbidden. However, both TBCP $\mathbb{G}_{n,ab}^T(\mathbf{k})$ and BCP $\mathbb{G}_{n,ab}^E(\mathbf{k})$ are \mathcal{T} even under time reversal operation and \mathcal{P} even under spatial inversion operation. That is to say $\mathcal{PT}\mathbb{G}_{n,ab}^{\text{T(E)}}(\mathbf{k}) = \mathbb{G}_{n,ab}^{\text{T(E)}}(\mathbf{k})$, indicating the TBCP and BCP remain nonzero under the symmetry of \mathcal{PT} . To more effectively illustrate the symmetry of transport coefficients across different mechanisms, Table I

TABLE I. The symmetry properties of the thermoelectric transport (a) coefficients of linear order, second-order extrinsic (induced by BCD) and second-order intrinsic (induced by BCP/TBCP) under spatial inversion (\mathcal{P}), time reversal (\mathcal{T}), and the combined operation of spatial and time reversal (\mathcal{PT}) are presented. The allowed (forbidden) conductivities are indicated by \checkmark (\times).

Order	contributions	response coefficients	\mathcal{P}	\mathcal{T}	\mathcal{PT}
linear	Drude ($\propto \tau^1$) [39]	$\sigma_{ab}^{\text{Drude}}$ $\alpha_{ab}^{\text{Drude}}$ $\kappa_{ab}^{\text{Drude}}$	\checkmark	\checkmark	\checkmark
	BC ($\propto \tau^0$) [1, 2]	σ_{ab}^{BC} α_{ab}^{BC} κ_{ab}^{BC}	\checkmark	\times	\times
second	Drude ($\propto \tau^2$) [3]	$\sigma_{abc}^{\text{Drude}}$ $\alpha_{abc}^{\text{Drude}}$ $\kappa_{abc}^{\text{Drude}}$	\times	\times	\checkmark
	BCD ($\propto \tau$) [8, 36]	$\sigma_{abc}^{\text{BCD}}$ $\alpha_{abc}^{\text{BCD}}$ $\kappa_{abc}^{\text{BCD}}$	\times	\checkmark	\times
	BCP ($\propto \tau^0$) [20] / TBCP ($\propto \tau^0$) in our work	$\sigma_{abc}^{\text{BCP}}$ α_{abc} κ_{abc}	\times	\times	\checkmark

summarizes the symmetries of linear and second-order transport coefficients induced by various contributions: the Drude, the BC, the BCD terms (τ -dependent), and BCP/TBCP terms (τ -independent). From the Table I, disregarding the Drude contribution (longitudinal, τ dependent), it is evident that the second-order intrinsic response plays a dominant role in systems with \mathcal{PT} symmetry.

To better understand and concretize the effect of intrinsic mechanism on nonlinear transport (no extrinsic mechanisms, only exists our proposed intrinsic mechanism), we consider a four-band Dirac model with \mathcal{PT} symmetry [20, 47]

$$\mathcal{H} = wk_x + v_x k_x \tau_x + v_y k_y \tau_y \sigma_x + \Delta \tau_z, \quad (17)$$

where (k_x, k_y) is the wave vector, the τ 's and σ 's are two sets of Pauli matrices, and w and 2Δ represent the tilt of energy band and the magnitude of gap, respectively. The parameters v_x, v_y and Δ are real. The energy spectrum is given by

$$\varepsilon_{\pm, \mathbf{k}} = wk_x \pm E_0(\mathbf{k}), \quad (18)$$

where \pm denotes the conduction and valence bands, and $E_0(\mathbf{k}) = \sqrt{\Delta^2 + k_x^2 v^2 + k_y^2 v^2}$ represents the energy splitting between the two bands. The \mathcal{PT} operation is expressed as $-i\sigma_y K$, where K corresponds to a complex conjugation. By applying the \mathcal{PT} operation, it can be confirmed that $\mathcal{PT}\mathcal{H}(\mathcal{PT})^{-1} = \mathcal{H}$, thereby demonstrating the fulfillment of \mathcal{PT} symmetry. Consequently, each energy band is required to be doubly degenerate [47].

In this model, $n = 1, 2$ are for valence bands and $n = 3, 4$ are for conduction bands. The analytical expression of the

TBCP for the valence band is evaluated from Eq. (6)

$$\mathbb{G}_1^T(\mathbf{k}) = \frac{wk_x v^4}{4E_0^5(\mathbf{k})} \begin{pmatrix} \frac{\Delta^2}{v^2} + k_y^2 & -k_x k_y \\ -k_x k_y & \frac{\Delta^2}{v^2} + k_x^2 \end{pmatrix}, \quad (19)$$

here, $v_x = v_y = v$ is assumed due to the isotropy in further analytical calculations. The TBCP of conduction and valence bands are opposite in sign, $\mathbb{G}_1^T(\mathbf{k}) = -\mathbb{G}_3^T(\mathbf{k})$. The TBCP elements $\mathbb{G}_{1,yy}^T(\mathbf{k})$, $\mathbb{G}_{3,yy}^T(\mathbf{k})$ and $\mathbb{G}_{1,xy}^T(\mathbf{k})$ on the (k_x, k_y) plane are depicted in Fig. 1(a)-(c), which are primarily concentrated around the gap region. The diagonal components of TBCP develop dipole-like structures [Fig.1(a) and (b)]; while the off-diagonal component exhibits a quadrupole-like structure in momentum space [Fig. 1(c)]. And $\mathbb{G}_{1,yy}^T(\mathbf{k}) = -\mathbb{G}_{3,yy}^T(\mathbf{k})$ is seen in Fig. 1(a) and Fig. 1(b). Apparently, it is evident that both $\mathbb{G}_{1,yy}^T(\mathbf{k})$ and $\mathbb{G}_{3,yy}^T(\mathbf{k})$ are odd functions of k_x ; while $\mathbb{G}_{1,xy}^T(\mathbf{k})$ in Fig. 1(c) is odd along the k_y axis, not k_x . Moreover, the integrand $\Lambda_{xyy}^-(\mathbf{k}) = \sum_{n=1,2} \Lambda_{xyy}^n(\mathbf{k})$ for second-order intrinsic thermal conductivity coefficient κ_{xyy} on the valence bands is displayed in Fig. 1(d), which is a combination of a monopole and a dipole along k_x .

The tilt term is important and induces non-zero TBCP and transport coefficients due to broken inversion symmetry. According to Eqs. (9) and (13), κ_{abc} and α_{abc} are both anti-symmetric with respect to first two indices, illustrating intrinsic Hall-type nature. As a result, only two independent components need to be considered: $\kappa_{xyy} = -\kappa_{yxy}$ and $\kappa_{xyx} = -\kappa_{yxx}$, with all other terms vanishing, and $\sigma_{abc}^{\text{BCP}}$ in Eq. (14) also satisfies the aforementioned conditions.

Taking xyy component as an example, we obtain the second-order intrinsic thermal conductivity coefficient con-

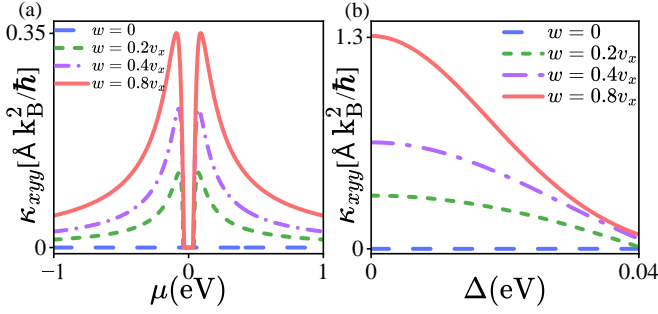


FIG. 2. (a) The thermal conductivity κ_{xyy} vs chemical potential μ , we set $\Delta = 40$ meV. (b) The thermal conductivity κ_{xyy} vs Δ , we set $\mu = 40$ meV. The other parameters are set to $v_x = v_y = 1$ eV \AA , $w/v_x = 0, 0.2, 0.4, 0.8$.

tributed by TBCP (see Appendix B for more details)

$$\kappa_{xyy} = -\frac{v\lambda\pi k_B^2 [\Delta^4\lambda^2(\lambda^2 - 1) + \Delta^2\mu^2 - \mu^4]}{48\hbar(\Delta^2\lambda^2 + \mu^2)^{5/2}}, \quad (20)$$

where $\lambda = w/v$ is dimensionless, determining the topology of the Fermi surface. It is noteworthy that our result contrasts with the findings reported in Ref [26], which is proportional to T^2 . This difference stems from the reason that the latter result is contributed by Berry curvature in the case that \mathcal{T} is preserved but inversion symmetry \mathcal{P} is broken.

Notably, κ_{xyy} is larger due to large TBCP around the band edges. Fig. 2(a) illustrates the relationship of κ_{xyy} and μ . Due to the ‘‘Fermi surface’’ effect, κ_{xyy} develops a peak rapidly and then decreases when μ enters into the edge of the band and gradually lifts up further. It is worth mentioning that κ_{xyy} is an even function of chemical potential μ , which means the conduction and valence bands make the same intrinsic contribution. Meanwhile, there is no the second-order thermal Hall conductivity in the absence of tilt term because of the inversion symmetry. In other words, the tilt term is the key condition to ensure the violation of space inversion along the direction of k_x , resulting in the non-vanishing κ_{xyy} . Furthermore, with the increase of w , κ_{xyy} rises as the degree of inversion symmetry breaking increases. In Fig. 2(b), the dependence of κ_{xyy} on Δ is shown. As Δ increases to match the chemical potential, κ_{xyy} gradually approaches zero but does not fully reach it, owing to the existence of the small quantity $\mathcal{O}(\lambda^2)$ in Eq. (20).

The second-order Nernst coefficient α_{xyy} vs μ is numerically computed in Fig. 3(a). There are two peaks but with opposite signs around the edge of valence and conduction bands respectively. Due to symmetry constraints, the BCD-induced $\sigma_{xyy}^{\text{BCD}}$ disappears under \mathcal{PT} symmetry. Drude-induced $\sigma_{xyy}^{\text{Drude}}$ is not considered, and we only consider BCP-induced $\sigma_{xyy}^{\text{BCP}}$. For a comparison, we plot the dependence of the second-order intrinsic conductivity $\sigma_{xyy}^{\text{BCP}}$ on μ in Fig. 3(b), where $\sigma_{xyy}^{\text{BCP}}$ decreases to zero as μ moves deeper into the conduction or valence bands. There are two peaks with opposite signs around the edges of valence bands and conduction bands, respectively.

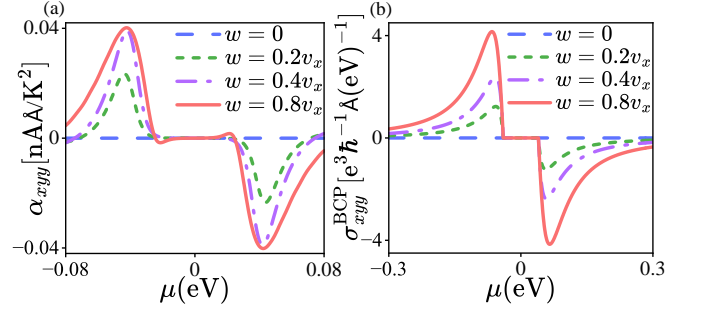


FIG. 3. (a) Nernst coefficient α_{xyy} vs μ , we set $k_B T = 2.6$ meV ($T \sim 30$ K). (b) Conductivity $\sigma_{xyy}^{\text{BCP}}$ vs μ . The parameters are set to $v_x = v_y = 1$ eV \AA , $\Delta = 40$ meV.

With these calculations, it is reasonable to analyze the ratio relationship between the second-order intrinsic thermal conductivity coefficient and the second-order intrinsic electrical conductivity coefficient (represented as σ_{xyy} for short). We can precisely obtain the second-order intrinsic Wiedemann-Franz law as

$$\kappa_{xyy} = -\frac{L}{2e} \left(\mu - \frac{\Delta^2\lambda^2}{\mu} \right) \sigma_{xyy}, \quad (21)$$

where L is the Lorentz number. Clearly, the second-order intrinsic thermal conductivity coefficient and second-order intrinsic conductivity coefficient are directly proportional to each other, and is determined by μ . The observed behavior stems from the different distributions of the TBCP [Fig. 1(a)-(c)], responsible for the thermal conductivity coefficient, and the BCP [20], which determines the electrical conductivity coefficient. This discrepancy in their distributions is likely the cause of the chemical potential μ -dependent nature of the proposed WF law. The second-order intrinsic WF law exhibits a direct proportionality between the second-order intrinsic thermal and electric transport, akin to the linear WF law. It differs from the second-order WF law due to the BCD mechanism ($\sigma_{abc} = -\frac{e}{2L} \frac{\partial \kappa_{abc}}{\partial \mu}$) [38], and it is tentatively ascribed to the disparity between the intrinsic and extrinsic mechanisms of the BCP and the BCD mechanism.

Until now the most of research had been focused on external contributions [8–11]. Since the proposal of the intrinsic NAHE [18], the intrinsic nonlinear current has drawn increasing attention as it assumes a dominant role in \mathcal{PT} -symmetric materials where the external contributions vanish. Recently, the impact of impurities and disorder in samples on transport effects has been explored [48–52]. However, it remains uncertain whether the second-order intrinsic transport phenomenon in \mathcal{PT} -symmetric materials is associated with impurities or disorder. Owing to its \mathcal{PT} symmetry, MnBi_2Te_4 [53–58] permits the presence of intrinsic NAHE, which has attracted extensive attention in recent years. To acquire an understanding of the magnitude of the second-order intrinsic thermoelectric response, MnBi_2Te_4 could be an ideal candidate material for detecting the proposed intrinsic second-order WF law and Nernst effect. It should be emphasized that the proposed intrinsic second-order WF law links the transverse thermal and

electric transport, thus is topologically dissipationless. Since the linear transverse WF law disappears, thus this intrinsic second-order transverse WF law is dominant. However, the longitudinal linear WF law still exists. Therefore, it leaves us an important open issue to explore the scaling relation between these two existing WF laws in the future.

ACKNOWLEDGMENTS

This work is supported by the National Key R&D Program of China (Grant No. 2024YFA1409200, No. 2022YFA1402802), CAS Project for Young Scientists in Basic Research Grant No. YSBR-057, the Strategic Priority Research Program of CAS (Grants No. XDB28000000, and No. XDB33000000), and the Training Program of Major Research plan of the National Natural Science Foundation of China (Grant No. 92165105).

Appendix A: The derivation of second-order intrinsic anomalous transport coefficients

1. The derivation of second-order intrinsic thermal conductivity coefficient

The second-order intrinsic thermal conductivity is κ_{abc} . By substituting the expressions $\tilde{\varepsilon}_{n,\mathbf{k}}$ and $\tilde{\Omega}_n(\mathbf{k})$ into the nonlinear anomalous thermal current, j_T^Q can be derived into

$$j_T^Q = -\frac{k_B^2 T}{\hbar} \nabla T \times \sum_m \int [d\mathbf{k}] \tilde{\Omega}_m(\mathbf{k}) \left[\frac{(\tilde{\varepsilon}_{m,\mathbf{k}} - \mu)^2}{(k_B T)^2} f_0^m + \frac{\pi^2}{3} - \ln^2(1 - f_0^m) - 2\text{Li}_2(1 - f_0^m) \right]. \quad (\text{A1})$$

In this paper, we mainly focus on the second-order transport phenomenon, which can be obtained by selectively collecting the terms proportional to $(\nabla T)^2$. Intrinsic second-order transverse thermal current in the direction a is given by

$$\begin{aligned} j_{T,a}^{Q(2)} &= \kappa_{abc} (-\nabla_b T) (-\nabla_c T) \\ &= -\frac{k_B^2 T}{\hbar} \sum_m \int [d\mathbf{k}] \left[\nabla T \times (\nabla \times \mathcal{A}_m^{(1)}(\mathbf{k})) \right]_a \left[\frac{(\varepsilon_{m,\mathbf{k}} - \mu)^2}{(k_B T)^2} f_0^m + \frac{\pi^2}{3} - \ln^2(1 - f_0^m) - 2\text{Li}_2(1 - f_0^m) \right] \\ &= \frac{k_B^2}{\hbar} \epsilon_{ab} \sum_m \int [d\mathbf{k}] \partial_a \mathbb{G}_{m,bc}^T(\mathbf{k}) \left[\frac{(\varepsilon_{m,\mathbf{k}} - \mu)^2}{(k_B T)^2} f_0^m + \frac{\pi^2}{3} - \ln^2(1 - f_0^m) - 2\text{Li}_2(1 - f_0^m) \right] (-\nabla_b T) (-\nabla_c T), \end{aligned} \quad (\text{A2})$$

where κ_{abc} is second-order thermal conductivity and $\left\{ \nabla T \times [\nabla \times \mathcal{A}_m^{(1)}(\mathbf{k})] \right\}_a = -\frac{1}{T} \epsilon_{ab} \partial_a \mathbb{G}_{m,bc}^T(\mathbf{k}) \nabla_b T \nabla_c T$ is used.

As a result, we can get second-order intrinsic thermal conductivity in Eq. (A2):

$$\kappa_{abc} = \frac{k_B^2}{\hbar} \epsilon_{ab} \sum_m \int [d\mathbf{k}] \partial_a \mathbb{G}_{m,bc}^T(\mathbf{k}) \left[\frac{(\varepsilon_{m,\mathbf{k}} - \mu)^2}{(k_B T)^2} f_0^m + \frac{\pi^2}{3} - \ln^2(1 - f_0^m) - 2\text{Li}_2(1 - f_0^m) \right]. \quad (\text{A3})$$

Considering the low temperature limit [30, 42], the first and third terms in square brackets cancel out in Eq. (A3), thus

$$\begin{aligned} \kappa_{abc} &= \frac{k_B^2}{\hbar} \epsilon_{ab} \sum_n \int [d\mathbf{k}] \partial_a \mathbb{G}_{n,bc}^T(\mathbf{k}) \left[\frac{\pi^2}{3} - 2\text{Li}_2(1 - f_0^n) \right] \\ &= \frac{\pi^2}{3} \frac{k_B^2}{\hbar} \epsilon_{ab} \sum_n \int [d\mathbf{k}] \partial_a \mathbb{G}_{n,bc}^T(\mathbf{k}) \theta(\mu - \varepsilon_{n,\mathbf{k}}) \\ &= \frac{\pi^2}{3} \frac{k_B^2}{\hbar} \epsilon_{ab} \sum_n \int [d\mathbf{k}] \mathbb{G}_{n,bc}^T(\mathbf{k}) \delta(\mu - \varepsilon_{n,\mathbf{k}}) \frac{\partial \varepsilon_{n,\mathbf{k}}}{\partial k_a} \\ &= \frac{\pi^2}{3} \frac{k_B^3 T}{\hbar} \epsilon_{ab} P_{a,bc}^T(\mu), \end{aligned} \quad (\text{A4})$$

where $\theta(\mu - \varepsilon_{n,\mathbf{k}})$ is step Function, $\text{Li}_2(0) = 0$, $\text{Li}_2(1) = \pi^2/6$, and we define $P_{a,bc}^T(\mu)$ as:

$$P_{a,bc}^T(\mu) = \frac{1}{k_B T} \sum_n \int [d\mathbf{k}] \mathbb{G}_{n,bc}^T(\mathbf{k}) \delta(\mu - \varepsilon_{n,\mathbf{k}}) \frac{\partial \varepsilon_{n,\mathbf{k}}}{\partial k_a}. \quad (\text{A5})$$

By partial integration, the existence of $\partial f_0^n / \partial \varepsilon_{n,\mathbf{k}}$ shows that the intrinsic nonlinear thermal current is related to the ‘‘Fermi-surface’’ effect, indicating that only the bands near the Fermi surface contribute to the integration, and is expected to be vanished in the band gap.

2. The derivation of second-order intrinsic Nernst coefficient

The second-order intrinsic Nernst coefficient is expressed by α_{abc} . By substituting the expressions $\tilde{\varepsilon}_{n,\mathbf{k}}$ and $\tilde{\Omega}_m(\mathbf{k})$ into the Nernst-like current, which is given by:

$$\mathbf{j}^N = -\frac{e}{\hbar} \nabla T \times \sum_m \int [d\mathbf{k}] \tilde{\Omega}_m(\mathbf{k}) \left[\frac{(\tilde{\varepsilon}_{m,\mathbf{k}} - \mu)}{T} f_0^m + k_B \ln(1 + e^{-\beta(\tilde{\varepsilon}_{m,\mathbf{k}} - \mu)}) \right], \quad (\text{A6})$$

thus, second-order intrinsic Nernst-like current in the a direction:

$$\begin{aligned} J_a^{N,(2)} &= \alpha_{abc} (-\nabla_b T) (-\nabla_c T) \\ &= -\frac{e}{\hbar} \sum_m \int [d\mathbf{k}] \left[\nabla T \times (\nabla \times \mathcal{A}_m^{(1)}(\mathbf{k})) \right]_a \left[\frac{\varepsilon_{m,\mathbf{k}} - \mu}{T} f_0^m + k_B \ln(1 + e^{-\beta(\varepsilon_{m,\mathbf{k}} - \mu)}) \right] \\ &= \frac{e}{\hbar T} \sum_m \int [d\mathbf{k}] \varepsilon_{ab} \partial_a \mathbb{G}_{m,bc}^T(\mathbf{k}) S_m(\mathbf{r}, \mathbf{k}) (-\nabla_b T) (-\nabla_c T), \end{aligned} \quad (\text{A7})$$

where $S_m(\mathbf{r}, \mathbf{k}) = \frac{(\varepsilon_{m,\mathbf{k}} - \mu)}{T} f_0^m + k_B \ln(1 + e^{-\beta(\varepsilon_{m,\mathbf{k}} - \mu)})$ is entropy density.

Furthermore, we obtain the second-order intrinsic Nernst coefficient α_{abc} in Eq. (A7),

$$\alpha_{abc} = \frac{e}{\hbar T} \varepsilon_{ab} \sum_m \int [d\mathbf{k}] \partial_a \mathbb{G}_{m,bc}^T(\mathbf{k}) S_m(\mathbf{r}, \mathbf{k}). \quad (\text{A8})$$

3. The derivation of second-order intrinsic Hall conductivity coefficient

The second-order intrinsic Hall conductivity reads σ_{abc} . The Berry curvature $\tilde{\Omega}_n^E(\mathbf{k})$ is corrected to first order in electric field \mathbb{E} : $\tilde{\Omega}_n^E(\mathbf{k}) = \Omega_n(\mathbf{k}) + \Omega_n^{E(1)}(\mathbf{k})$, $\Omega_n(\mathbf{k})$ is the unperturbed Berry curvature, $\Omega_n^{E(1)}(\mathbf{k})$ is the first-order correction to the Berry curvature $\Omega_n^{E(1)}(\mathbf{k}) = \nabla_{\mathbf{k}} \times \mathcal{A}_n^{E(1)}(\mathbf{k})$, where $\mathcal{A}_n^{E(1)}(\mathbf{k})$ is the first-order correction of electric field \mathbb{E} to the Berry connection, $\mathcal{A}_{n,a}^{E(1)}(\mathbf{k}) = \mathbb{G}_{n,ab}^E(\mathbf{k}) \mathbb{E}_b$, in which the BCP tensor [18] is defined as

$$\mathbb{G}_{n,ab}^E(\mathbf{k}) = 2e\Re \sum_{l \neq n} \frac{\mathcal{A}_{nl,a}(\mathbf{k}) \mathcal{A}_{ln,b}(\mathbf{k})}{\varepsilon_{n,\mathbf{k}} - \varepsilon_{l,\mathbf{k}}}. \quad (\text{A9})$$

Employing the Boltzmann equation, $\dot{\mathbf{k}} \cdot \nabla_{\mathbf{k}} f_{\mathbf{k}}^n = -\frac{f_{\mathbf{k}}^n - f_0^n}{\tau}$, the non-equilibrium distribution function can be obtained as:

$$f_{\mathbf{k}}^n = \sum_{m=0}^{\infty} \left(\frac{e\tau}{\hbar} \mathbf{E} \cdot \nabla_{\mathbf{k}} \right)^m f_0^n, \quad (\text{A10})$$

The a -direction component of the second-order current $\mathbf{j}^{E,(2)}$ is denoted as $j_a^{E,(2)} = \sigma_{abc} E_b E_c$. Subsequently, the second-order conductivity can be divided into three parts [8, 18, 20, 21, 24, 45]: $\sigma_{abc} = \sigma_{abc}^{\text{Drude}} + \sigma_{abc}^{\text{BCP}} + \sigma_{abc}^{\text{BCD}}$, with

$$\sigma_{abc}^{\text{BCP}} = -\frac{e^2}{\hbar} \varepsilon_{ab} \sum_m \int [d\mathbf{k}] \partial_a \mathbb{G}_{m,bc}^E(\mathbf{k}) f_0^m. \quad (\text{A11})$$

In this context, we have only analyzed the second-order electrical conductivity contributed by BCP, utilizing the Sommerfeld expansion [39],

$$\int_{-\infty}^{+\infty} d\varepsilon \frac{\partial f_0^n}{\partial \varepsilon} \Phi(\varepsilon) = -\Phi(\mu) - \frac{\pi^2}{6} k_B^2 T^2 \left[\frac{\partial^2 \Phi(\varepsilon)}{\partial \varepsilon^2} \right] \Big|_{\varepsilon=\mu} - \frac{7\pi^4}{360} k_B^4 T^4 \left[\frac{\partial^4 \Phi(\varepsilon)}{\partial \varepsilon^4} \right] \Big|_{\varepsilon=\mu}, \quad (\text{A12})$$

we can simplify Eq. (A11) to Eq. (A13),

$$\begin{aligned} \sigma_{abc}^{\text{BCP}} &= -\frac{e^2}{\hbar} \varepsilon_{ab} \sum_n \int [d\mathbf{k}] \partial_a \mathbb{G}_{n,bc}^E(\mathbf{k}) f_0^n \\ &= \frac{e^3}{\hbar} \varepsilon_{ab} \int d\varepsilon \left\{ \frac{1}{e} \int \sum_n [d\mathbf{k}] \mathbb{G}_{n,bc}^E(\mathbf{k}) \delta(\varepsilon - \varepsilon_{n,\mathbf{k}}) \frac{\partial \varepsilon_{n,\mathbf{k}}}{\partial k_a} \right\} \frac{\partial f_0^n}{\partial \varepsilon} \\ &= -\frac{e^3}{\hbar} \varepsilon_{ab} \left[P_{a,bc}^E(\mu) + \frac{\pi^2}{6} (k_B T)^2 P_{a,bc}^{E(2)}(\mu) \right], \end{aligned} \quad (\text{A13})$$

where, $P_{a,bc}^{E(n)}(\mu) = \partial^n P_{a,bc}^E(\mu)/\partial\mu^n$, and $P_{a,bc}^E(\mu)$ is defined as

$$P_{a,bc}^E(\mu) = \frac{1}{e} \int \sum_n [d\mathbf{k}] \mathbb{G}_{n,bc}^E(\mathbf{k}) \delta(\mu - \varepsilon_{n,\mathbf{k}}) \frac{\partial \varepsilon_{n,\mathbf{k}}}{\partial k_a}. \quad (\text{A14})$$

Appendix B: The derivation of the second-order intrinsic Wiedemann-Franz law

From Eqs. (A4) and (19), we can obtain the second-order intrinsic thermal conductivity coefficient for the valence band,

$$\begin{aligned} \kappa_{xyy} &= \frac{\pi^2}{3} \frac{k_B^3 T}{\hbar} \epsilon_{xy} P_{x,yy}^\Gamma(\mu) \\ &= \frac{\pi^2}{3} \frac{k_B^3 T}{\hbar} \frac{1}{k_B T} \int [d\mathbf{k}] \left[\mathbb{G}_{1,yy}^\Gamma(\mathbf{k}) \frac{\partial \varepsilon_{1,\mathbf{k}}}{\partial k_x} - \mathbb{G}_{1,xy}^\Gamma(\mathbf{k}) \frac{\partial \varepsilon_{1,\mathbf{k}}}{\partial k_y} \right] \delta(\varepsilon_{1,\mathbf{k}} - \mu) \\ &= \frac{\pi^2}{3} \frac{k_B^3 T}{\hbar} \frac{1}{(2\pi)^2 k_B T} \int \int dk_x dk_y \left[-\frac{w^2 k_x v^2}{4E_0^5(\mathbf{k})} (\Delta^2 + k_x^2 v^2) + \frac{w v^4 k_x^2 E_0(\mathbf{k})}{4E_0^5(\mathbf{k})} \right] \delta[wk_x - E_0(\mathbf{k}) - \mu]. \end{aligned} \quad (\text{B1})$$

We can incorporate the v factor into k_x and k_y by redefining k_x as k_x/v and k_y as k_y/v , providing a more convenient form for subsequent calculations and analysis. Then from the $\delta[wk_x - E_0(\mathbf{k}) - \mu]$ function in Eq. (B1), we can get

$$k_y = \pm \sqrt{(\mu - \lambda k_x)^2 - \Delta^2 - k_x^2}, \quad (\text{B2})$$

and the range of k_x is given by $k_x \in [k_a, k_b]$ on the Fermi surface, where the values of k_a and k_b are expressed as $k_{a/b} = \frac{-\mu\lambda \mp \sqrt{\mu^2 - \Delta^2 + \lambda^2 \Delta^2}}{1 - \lambda^2}$.

Therefore, the second-order intrinsic thermal conductivity coefficient κ_{xyy} for the conduction bands in Eq. (B1) by using the method in [20] is written as :

$$\begin{aligned} \kappa_{xyy} &= \frac{\pi^2}{3} \frac{k_B^2}{\hbar} \frac{v\lambda}{(2\pi)^2} \int_{k_a}^{k_b} dk_x \left[\frac{k_x^2(\lambda k_x - \mu) - \lambda k_x(\Delta^2 + k_x^2)}{4(\lambda k_x - \mu)^5} \right] \frac{2(\lambda k_x - \mu)}{|k_y|} \Bigg|_{k_y = \pm \sqrt{(\mu - \lambda k_x)^2 - \Delta^2 - k_x^2}} \\ &= \frac{\pi^2}{3} \frac{k_B^2}{\hbar} \frac{v\lambda}{8\pi^2} \int_{k_a}^{k_b} dk_x \frac{k_x^2(\lambda k_x - \mu) - \lambda k_x(\Delta^2 + k_x^2)}{(\lambda k_x - \mu)^4} \frac{1}{\sqrt{(\mu - \lambda k_x)^2 - \Delta^2 - k_x^2}} \\ &= -\frac{v\lambda\pi k_B^2}{48\hbar} \frac{[\Delta^4 \lambda^2 (\lambda^2 - 1) + \Delta^2 \mu^2 - \mu^4]}{(\Delta^2 \lambda^2 + \mu^2)^{5/2}}, \end{aligned} \quad (\text{B3})$$

where $\lambda = w/v$, quantifying the magnitude of band tilting.

For the second-order intrinsic Hall conductivity coefficient σ_{xyy} , only the influence of BCP mechanism on the coefficient is considered, the analytical expression of σ_{xyy} is given in Ref. [20], which is

$$\sigma_{xyy} = -\frac{e^3 v \lambda \mu [\Delta^2 (\lambda^2 - 1) + \mu^2]}{8\pi \hbar (\Delta^2 \lambda^2 + \mu^2)^{5/2}}, \quad (\text{B4})$$

and for the conduction bands, the identical result in Eqs. (B1) and (B4) can be achieved.

Therefore, by synthesizing the results obtained above, we can successfully derive the second-order intrinsic Wiedemann-Franz law,

$$\kappa_{xyy} = -\frac{L}{2e} \left(\mu - \frac{\Delta^2 \lambda^2}{\mu} \right) \sigma_{xyy} \quad (\text{B5})$$

- tronic properties, *Rev. Mod. Phys.* **82**, 1959 (2010).
- [3] S. S. Tsirkin and I. Souza, On the separation of Hall and Ohmic nonlinear responses, *SciPost Phys. Core* **5**, 039 (2022).
- [4] Y. Wang, Z. Zhang, Z.-G. Zhu, and G. Su, Intrinsic nonlinear ohmic current, *Phys. Rev. B* **109**, 085419 (2024).
- [5] D. Kaplan, T. Holder, and B. Yan, Unification of nonlinear anomalous Hall effect and nonreciprocal magnetoresistance in metals by the quantum geometry, *Phys. Rev. Lett.* **132**, 026301 (2024).
- [6] J. Jia, L. Xiang, Z. Qiao, and J. Wang, On the equivalence of the semiclassical theory and the response theory, (2024), [arXiv:2404.17086 \[cond-mat.mes-hall\]](https://arxiv.org/abs/2404.17086).
- [7] T. Nag, S. K. Das, C. Zeng, and S. Nandy, Third-order hall effect in the surface states of a topological insulator, *Phys. Rev. B* **107**, 245141 (2023).
- [8] I. Sodemann and L. Fu, Quantum nonlinear Hall effect induced by Berry curvature dipole in time-reversal invariant materials, *Phys. Rev. Lett.* **115**, 216806 (2015).
- [9] Z. Du, C. Wang, H.-Z. Lu, and X. Xie, Band signatures for strong nonlinear Hall effect in bilayer WTe_2 , *Phys. Rev. Lett.* **121**, 266601 (2018).
- [10] Q. Ma, S.-Y. Xu, H. Shen, D. MacNeill, V. Fatemi, T.-R. Chang, A. M. Mier Valdivia, S. Wu, Z. Du, C.-H. Hsu, S. Fang, Q. D. Gibson, K. Watanabe, T. Taniguchi, R. J. Cava, E. Kaxiras, H.-Z. Lu, H. Lin, L. Fu, N. Gedik, and P. Jarillo-Herrero, Observation of the nonlinear Hall effect under time-reversal-symmetric conditions, *Nature* **565**, 337 (2018).
- [11] R.-C. Xiao, D.-F. Shao, W. Huang, and H. Jiang, Electrical detection of ferroelectriclike metals through the nonlinear Hall effect, *Phys. Rev. B* **102**, 024109 (2020).
- [12] C. Zeng, S. Nandy, and S. Tewari, Nonlinear transport in Weyl semimetals induced by Berry curvature dipole, *Phys. Rev. B* **103**, 245119 (2021).
- [13] Y. Zhang, Y. Sun, and B. Yan, Berry curvature dipole in Weyl semimetal materials: An ab initio study, *Phys. Rev. B* **97**, 041101 (2018).
- [14] C. Wang, R.-C. Xiao, H. Liu, Z. Zhang, S. Lai, C. Zhu, H. Cai, N. Wang, S. Chen, Y. Deng, Z. Liu, S. A. Yang, and W.-B. Gao, Room-temperature third-order nonlinear Hall effect in Weyl semimetal TaIrTe_4 , *Natl. Sci. Rev.* **9**, nwac020 (2022).
- [15] C.-P. Zhang, J. Xiao, B. T. Zhou, J.-X. Hu, Y.-M. Xie, B. Yan, and K. T. Law, Giant nonlinear Hall effect in strained twisted bilayer graphene, *Phys. Rev. B* **106**, L041111 (2022).
- [16] S. Akatsuka, M. Sakano, T. Yamamoto, T. Nomoto, R. Arita, R. Murata, T. Sasagawa, K. Watanabe, T. Taniguchi, N. Miitsuishi, M. Kitamura, K. Horiba, K. Sugawara, S. Souma, T. Sato, H. Kumigashira, K. Shinokita, H. Wang, K. Matsuda, S. Masubuchi, T. Machida, and K. Ishizaka, 180° -twisted bilayer ReSe_2 as an artificial noncentrosymmetric semiconductor, *Phys. Rev. Research* **6**, 1022048 (2024).
- [17] H. Pang, G. Jin, and L. He, Tuning of Berry-curvature dipole in taas slabs: An effective route to enhance the nonlinear Hall response, *Phys. Rev. Materials* **8**, 043403 (2024).
- [18] Y. Gao, S. A. Yang, and Q. Niu, Field induced positional shift of bloch electrons and its dynamical implications, *Phys. Rev. Lett.* **112**, 166601 (2014).
- [19] Y. Gao, S. A. Yang, and Q. Niu, Geometrical effects in orbital magnetic susceptibility, *Phys. Rev. B* **91**, 214405 (2015).
- [20] H. Liu, J. Zhao, Y.-X. Huang, W. Wu, X.-L. Sheng, C. Xiao, and S. A. Yang, Intrinsic second-order anomalous Hall effect and its application in compensated antiferromagnets, *Phys. Rev. Lett.* **127**, 277202 (2021).
- [21] C. Wang, Y. Gao, and D. Xiao, Intrinsic nonlinear Hall effect in antiferromagnetic tetragonal CuMnAs , *Phys. Rev. Lett.* **127**, 277201 (2021).
- [22] H. Liu, J. Zhao, Y.-X. Huang, X. Feng, C. Xiao, W. Wu, S. Lai, W.-b. Gao, and S. A. Yang, Berry connection polarizability tensor and third-order Hall effect, *Phys. Rev. B* **105**, 045118 (2022).
- [23] O. Pal and T. K. Ghosh, Polarization and third-order Hall effect in III-V semiconductor heterojunctions, *Phys. Rev. B* **109**, 035202 (2024).
- [24] Z.-F. Zhang, Z.-G. Zhu, and G. Su, Symmetry dictionary on charge and spin nonlinear responses for all magnetic point groups with nontrivial topological nature, *Natl. Sci. Rev.* **10**, nwad104 (2023).
- [25] J.-C. Li and Z.-G. Zhu, Intrinsic second-order magnon thermal Hall effect, *J. Phys. Condens. Matter* **36**, 395802 (2024).
- [26] D.-K. Zhou, Z.-F. Zhang, X.-Q. Yu, Z.-G. Zhu, and G. Su, Fundamental distinction between intrinsic and extrinsic nonlinear thermal Hall effects, *Phys. Rev. B* **105**, 1201103 (2022).
- [27] X.-Q. Yu, Z.-G. Zhu, and G. Su, Hexagonal warping induced nonlinear planar Nernst effect in nonmagnetic topological insulators, *Phys. Rev. B* **103**, 035410 (2021).
- [28] M. Saha and D. Chowdhury, Anomalous thermoelectric properties of a Floquet topological insulator with spin momentum non-orthogonality, *J. Appl. Phys.* **122**, 174301 (2017).
- [29] T. Choudhari and N. Deo, Effect of hexagonal warping of the Fermi surface on the thermoelectric properties of a topological insulator irradiated with linearly polarized radiation, *Phys. Rev. B* **100**, 035303 (2019).
- [30] A. Roy Karmakar, S. Nandy, A. Taraphder, and G. P. Das, Giant anomalous thermal Hall effect in tilted type-I magnetic Weyl semimetal $\text{Co}_3\text{Sn}_2\text{S}_2$, *Phys. Rev. B* **106**, 245133 (2022).
- [31] S. Nandy, A. Taraphder, and S. Tewari, Planar thermal Hall effect in Weyl semimetals, *Phys. Rev. B* **100**, 115139 (2019).
- [32] T. M. McCormick, R. C. McKay, and N. Trivedi, Semiclassical theory of anomalous transport in type-II topological Weyl semimetals, *Phys. Rev. B* **96**, 235116 (2017).
- [33] P. Bhalla, Intrinsic contribution to nonlinear thermoelectric effects in topological insulators, *Phys. Rev. B* **103**, 115304 (2021).
- [34] Y. Wang, Z.-G. Zhu, and G. Su, Field-induced Berry connection and anomalous planar Hall effect in tilted Weyl semimetals, *Phys. Rev. Research* **5**, 043156 (2023).
- [35] X.-B. Qiang, Z. Z. Du, H.-Z. Lu, and X. C. Xie, Topological and disorder corrections to the transverse Wiedemann-Franz law and Mott relation in kagome magnets and Dirac materials, *Phys. Rev. B* **107**, 1161302 (2023).
- [36] C. Zeng, S. Nandy, and S. Tewari, Fundamental relations for anomalous thermoelectric transport coefficients in the nonlinear regime, *Phys. Rev. Research* **2**, 032066 (2020).
- [37] K. Nakata, Y. Ohnuma, and S. K. Kim, Violation of the magnonic Wiedemann-Franz law in the strong nonlinear regime, *Phys. Rev. B* **105**, 184409 (2022).
- [38] Y. Wang, Z.-G. Zhu, and G. Su, Quantum theory of nonlinear thermal response, *Phys. Rev. B* **106**, 035148 (2022).
- [39] N. W. Ashcroft, J. A. Mermin, and N. David, *Solid State Physics* (Brooks Cole; New edition (2 Jan. 1976), 1976).
- [40] L. Smrcka and P. Streda, Transport coefficients in strong magnetic fields, *J. Phys. C: Solid State Phys.* **10**, 2153 (1977).
- [41] Z. Z. Du, H.-Z. Lu, and X. C. Xie, Nonlinear Hall effects, *Nat. Rev. Phys.* **3**, 744 (2021).
- [42] T. Yokoyama and S. Murakami, Transverse magnetic heat transport on the surface of a topological insulator, *Phys. Rev. B* **83**, 161407 (2011).
- [43] D. L. Bergman and V. Oganesyan, Theory of dissipationless Nernst effects, *Phys. Rev. Lett.* **104**, 066601 (2010).

- [44] D. Xiao, Y. Yao, Z. Fang, and Q. Niu, Berry-phase effect in anomalous thermoelectric transport, *Phys. Rev. Lett.* **97**, 026603 (2006).
- [45] D. Kaplan, T. Holder, and B. Yan, Unifying semiclassical and quantum perturbation theory at nonlinear order, *SciPost Phys.* **14**, 082 (2023).
- [46] S. Lai, H. Liu, Z. Zhang, J. Zhao, X. Feng, N. Wang, C. Tang, Y. Liu, K. S. Novoselov, S. A. Yang, and W.-b. Gao, Third-order nonlinear Hall effect induced by the Berry-connection polarizability tensor, *Nat. Nanotechnol.* **16**, 869 (2021).
- [47] P. Tang, Q. Zhou, G. Xu, and S.-C. Zhang, Dirac fermions in an antiferromagnetic semimetal, *Nat. Phys.* **12**, 1100 (2016).
- [48] N. A. Sinitsyn, Q. Niu, J. Sinova, and K. Nomura, Disorder effects in the anomalous Hall effect induced by Berry curvature, *Phys. Rev. B* **72**, 045346 (2005).
- [49] Z. Z. Du, C. M. Wang, S. Li, H.-Z. Lu, and X. C. Xie, Disorder-induced nonlinear Hall effect with time-reversal symmetry, *Nat. Commun.* **10**, 3047 (2019).
- [50] R. B. Atencia, D. Xiao, and D. Culcer, Disorder in the nonlinear anomalous Hall effect of PT-symmetric dirac fermions, *Phys. Rev. B* **108**, 1201115 (2023).
- [51] Y. Arai, J. Hayashi, K. Takeda, H. Tou, H. Sugawara, and H. Kotegawa, Intrinsic anomalous Hall effect arising from antiferromagnetism as revealed by high-quality NbMnP, *J. Phys. Soc. Jpn.* **93**, 063702 (2024).
- [52] L. Ding, J. Koo, L. Xu, X. Li, X. Lu, L. Zhao, Q. Wang, Q. Yin, H. Lei, B. Yan, Z. Zhu, and K. Behnia, Intrinsic anomalous Nernst effect amplified by disorder in a half-metallic semimetal, *Phys. Rev. X* **9**, 041061 (2019).
- [53] A. Gao, Y.-F. Liu, J.-X. Qiu, B. Ghosh, T. V. Trevisan, Y. Onishi, C. Hu, T. Qian, H.-J. Tien, S.-W. Chen, M. Huang, D. Bérubé, H. Li, C. Tzschaschel, T. Dinh, Z. Sun, S.-C. Ho, S.-W. Lien, B. Singh, K. Watanabe, T. Taniguchi, D. C. Bell, H. Lin, T.-R. Chang, C. R. Du, A. Bansil, L. Fu, N. Ni, P. P. Orth, Q. Ma, and S.-Y. Xu, Quantum metric nonlinear Hall effect in a topological antiferromagnetic heterostructure, *Science* **381**, 181 (2023).
- [54] Y. Deng, Y. Yu, M. Z. Shi, Z. Guo, Z. Xu, J. Wang, X. H. Chen, and Y. Zhang, Quantum anomalous Hall effect in intrinsic magnetic topological insulator MnBi_2Te_4 , *Science* **367**, 895 (2020).
- [55] H. Li, C. Zhang, C. Zhou, C. Ma, X. Lei, Z. Jin, H. He, B. Li, K. T. Law, and J. Wang, Quantum geometry quadrupole-induced third-order nonlinear transport in antiferromagnetic topological insulator MnBi_2Te_4 , *Nat. Commun.* **15**, 7779 (2024).
- [56] K. He, MnBi_2Te_4 -family intrinsic magnetic topological materials, *npj Quantum Materials* **5**, 90 (2020).
- [57] W. Lin, Y. Feng, Y. Wang, J. Zhu, Z. Lian, H. Zhang, H. Li, Y. Wu, C. Liu, Y. Wang, J. Zhang, Y. Wang, C.-Z. Chen, X. Zhou, and J. Shen, Direct visualization of edge state in even-layer MnBi_2Te_4 at zero magnetic field, *Nat. Commun.* **13**, 7714 (2022).
- [58] S. Li, T. Liu, C. Liu, Y. Wang, H.-Z. Lu, and X. C. Xie, Progress on the antiferromagnetic topological insulator MnBi_2Te_4 , *Natl. Sci. Rev.* **11**, nwac296 (2023).